ACS NANO

www.acsnano.org

ARTICLE

Hybridization of Biomolecular Crystals and Low-Dimensional Materials

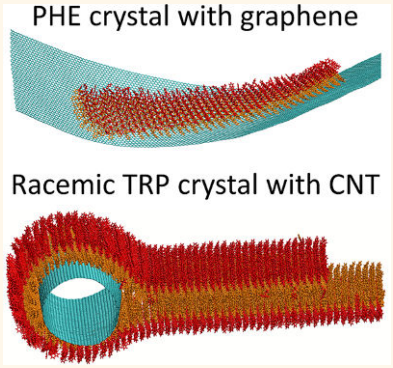
Pavel Rehak and Petr Král*

Cite This: *ACS Nano* 2021, 15, 6678–6683

Read Online

ACCESS | Metrics & More | Article Recommendations | Supporting Information

ABSTRACT: **In cellular environments, metabolites, peptides, proteins, and other biomolecules can self-assemble into planar and fibrilar molecular crystals. We use atomistic molecular dynamics simulations to show that such biomolecular crystals coupled with low-dimensional materials can form stable hybrid superstructures. We discuss enantiopure and racemic TRP and PHE amino acid crystals adsorbed on or intercalated between graphene, phosphorene, and carbon nanotubes. While racemic biomolecular crystals tend to stay straight in solutions and when adsorbed on flat and cylindrical nanosurfaces, enantiopure crystals undergo twisting. Mixed material properties of these hybrid superstructures can be attractive in many applications.**



KEYWORDS: *graphene, phosphorene, CNT, tryptophan, phenylalanine, enantiopure crystal, racemic crystal*

Downloaded via UNIV OF ILLINOIS CHICAGO on April 30, 2021 at 05:15:16 (UTC).
See https://pubs.acs.org/sharingguidelines for options on how to legitimately share published articles.

Amyloid peptides, various metabolites, and other biomolecules can form planar and fibrillar crystals in cellular biosystems.[1−6] These biomolecular crystals adsorbed on low-dimensional materials or intercalated between them could form hybrid materials.[7−10] Individual solvated biomolecules can easily adsorb on material surfaces.[11−22] For example, amino acids, peptides, and nucleobases couple to nanocarbons by a $\pi-\pi$ stacking of their aromatic groups. Graphene and hydrophobic nanoparticles can also be intercalated in biological membranes.[23,24] Moreover, graphene and carbon nanotubes can sense proteins and nucleic acids adsorbed on them.[25−27] When molecular crystals are coupled with low-dimensional materials, each of the components could provide different properties to the hybrid materials.

Here, we use atomistic molecular dynamics (MD) simulations to study complexation of biomolecular crystals and low-dimensional materials, mostly provided by a van der Waals (vdW) coupling.[28] We consider enantiopure and racemic crystals of tryptophan (TRP) and phenylalanine (PHE),[29−31] which have indole and phenyl side groups, respectively. We study hybrid nanostructures formed by such biomolecular crystals adsorbed on graphene, phosphorene, and carbon nanotubes or intercalated in graphene cells. These materials could be used in optics, electronics, and biocompatible applications.

RESULTS AND DISCUSSION

Biomolecular Crystals on Planar Nanosurfaces. Metabolite crystals can form in physiological solutions, be extracted, and be placed on various substrates. Initially, we prepared (Methods) a small L-TRP single bilayer crystal (L-TRP-C)[30] and placed it on graphene and phosphorene sheets, as shown in Figure 1a,b and c,d, respectively. These systems were simulated for 100 ns in vacuum at T = 310 K. The biomolecular crystals translated by diffusion on both nanosurfaces, but their motion was more constrained on phosphorene due to its unidirectional grooves (Figure 1d). Other systems with L-TRP-C on graphene and phosphorene in vacuum were also simulated (Figures S1 and S2, movie 1).

When L-TRP-C, elongated along its aromatic zipper, was simulated in a physiological solution, it twisted (Figure 2a), signaling that it might form fibrils.[32,33] Therefore, we simulated this L-TRP-C on graphene nanoribbons in a physiological solution (Figure 2b,g). It twisted (100 ns) much less on these nanosurfaces, most likely due to their relative rigidity (Movie 2). Moreover, only several amino acids left these crystals. Similar behavior was observed in this L-TRP-C on a relatively small graphene nanoribbon in a physiological solution (Figure S3). To promote a crystal twisting, we simulated L-TRP-C on deformed surfaces of CNTs[8] (below).

Received: November 30, 2020
Accepted: March 30, 2021
Published: April 5, 2021



© 2021 American Chemical Society

https://doi.org/10.1021/acsnano.0c10027
ACS Nano 2021, 15, 6678–6683

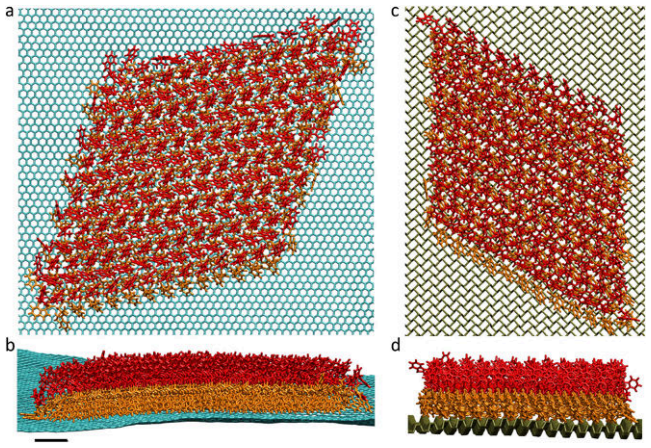


Figure 1. (a, b) L-TRP-C (14 × 14 × 2 amino acids) adsorbed in vacuum on a graphene sheet (16.0 × 22.8 nm^2) after 100 ns simulations (top and side views). (c, d) L-TRP-C (12 × 12 × 2 amino acids) adsorbed in vacuum on a phosphorene sheet (14.8 × 19.7 nm^2) at 100 ns. Scale bar is 1 nm.

A bilayer racemic (achiral) TRP crystal (A-TRP-C) freely simulated (20 ns) in a physiological solution manifested only small bending fluctuations, irrespective of its cutting (Figure 2c).[33] When the solvated A-TRP-C with the long axis parallel to the aromatic zipper was simulated (100 ns) on the graphene nanoribbon, it remained planar without significant bending fluctuations (Figure 2d). In contrast, a freely solvated L-PHE-C cut orthogonal to the zipper was significantly twisting[33] (Figure 2e). When this L-PHE-C was simulated (100 ns) on a graphene nanoribbon, the whole heterostructure became twisted (Figure 2f). The hybrid nanostructure became helical, which could provide it an optical activity in CD spectra. However, L-PHE-C with the parallel cut (Supporting Information) remained relatively flat and only slightly cracked on the graphene nanoribbon (Figure S4 and Movie 3).

Biomolecular Crystals on Carbon Nanotubes. Next, we studied the adsorption of biomolecular crystals on CNTs submerged in a physiological solution. First, (35,35) CNT was placed 2−4 Å above the center of L-TRP-C and parallel to its aromatic zipper, as shown in Figure 3a. The adsorption of L-TRP-C on CNT occurred in steps, determined by the initial configurations (Figure S5, Movie 4, and Movie 5). Parts b and c of Figure 3 show that L-TRP-C wrapped smoothly around CNT within 417 ns (Movie 5) without being significantly damaged. However, all enantiopure L-TRP-Cs twisted on

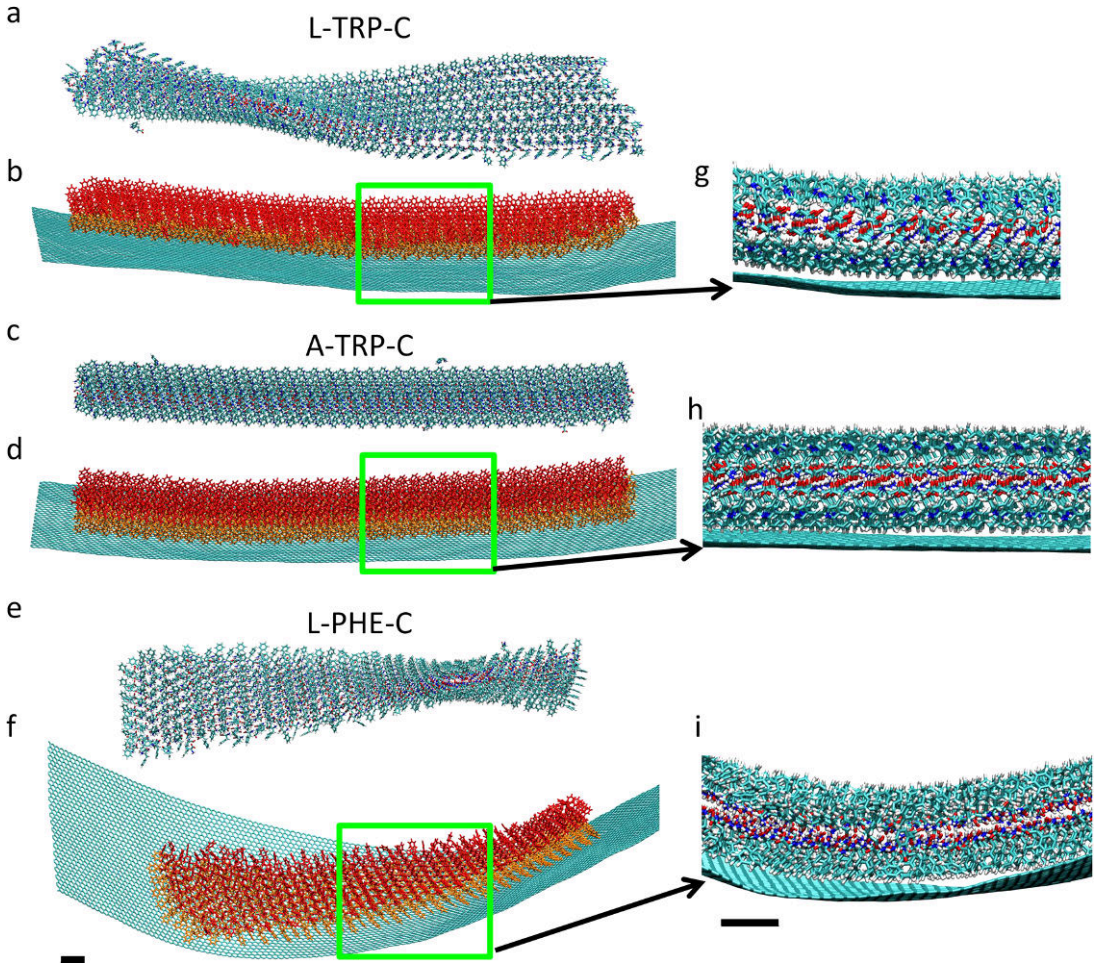


Figure 2. L-TRP-C (40 × 8 × 2 amino acids): (a) freely solvated in a physiological solution at 20 ns and (b) adsorbed on a graphene nanoribbon (7.9 × 28.9 nm^2) at 100 ns. (c) A-TRP-C (40 × 8 × 2 amino acids) freely solvated at 20 ns and (d) adsorbed on a graphene nanoribbon from (b) at 100 ns. (e) L-PHE-C (8 × 40 × 2 amino acids) freely solvated and (f) adsorbed on a graphene nanoribbon from (b) at 100 ns. (g−i) Magnified views of L-TRP-C, A-TRP-C, and L-PHE-C on graphene nanoribbons in physiological solution. Scale bars are 1 nm.

https://doi.org/10.1021/acsnano.0c10027
ACS Nano 2021, 15, 6678−6683

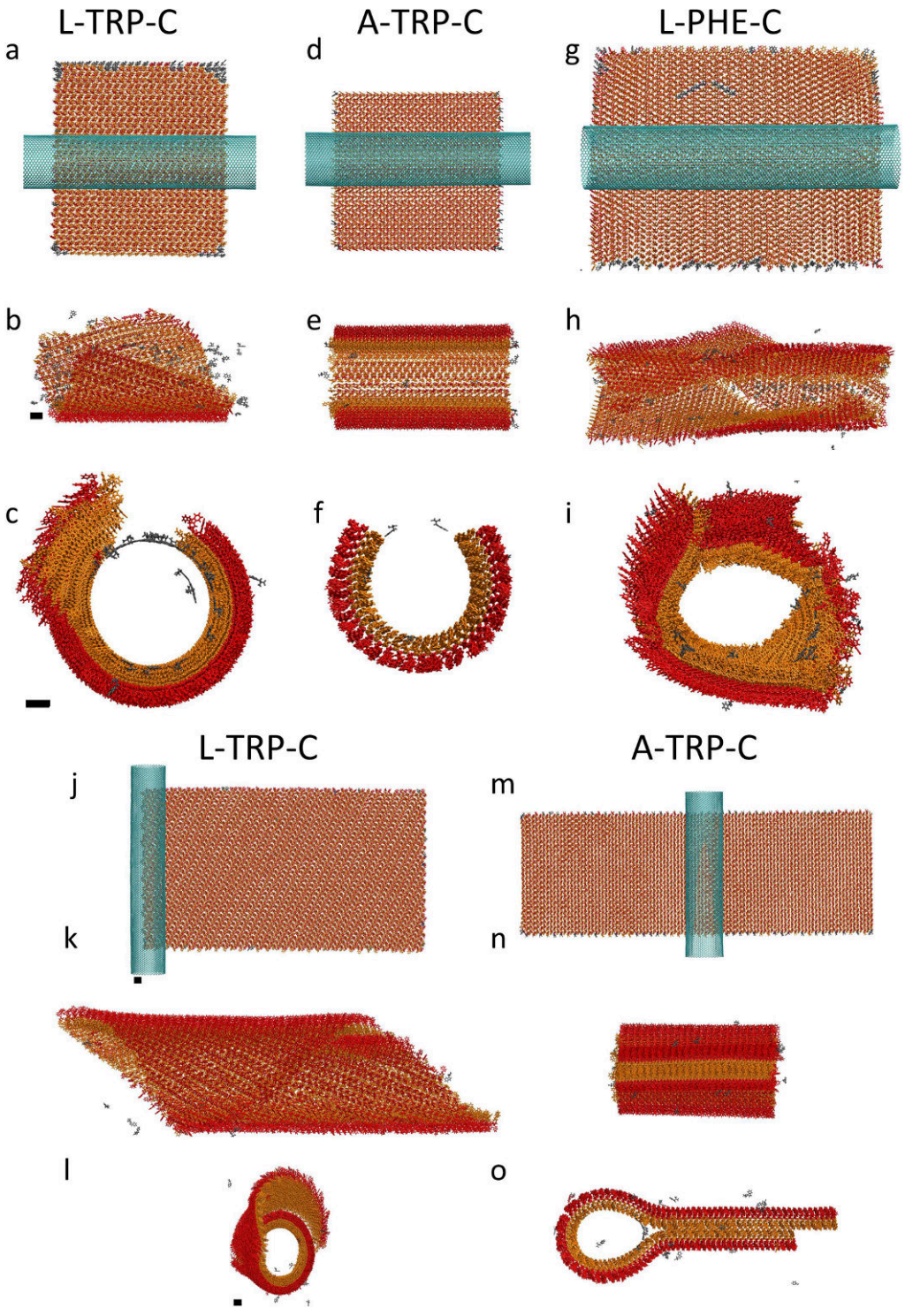


Figure 3. (a–c) (35,35) CNT (18.8 nm long) was placed at the center of L-TRP-C (48 × 34 × 2 amino acids) and simulated for 417 ns (top, start; middle and bottom, CNT not shown). (d–f) This CNT was placed above the center of A-TRP-C (48 × 34 × 2 amino acids) and simulated for just 15 ns. (g–i) (35,35) CNT (21 nm long) was placed above the center of L-PHE-C (34 × 48 × 2 amino acids) and simulated for 94 ns. (j–l) (35,35) CNT (24.0 nm long) placed on side of L-TRP-C (18 × 69 × 2 amino acids) and simulated for 48 ns. (m–o) (35,35) CNT (18.8 nm long) placed in center of A-TRP-C (24 × 102 × 2 amino acids) and simulated for 51 ns. Scale bars represent 1 nm.

CNTs in the same helical fashion (Figure S5), like the freely solvated L-TRP-Cs in Figure 2a.

We have also simulated the adsorption of A-TRP-C on (35,35) CNT aligned along the aromatic zipper. When this CNT was placed above the center of A-TRP-C, the crystal neatly folded around this CNT within 15 ns, as shown in Figure 3d–f (Figure S6, Movie 6). Molecular crystals adsorbed on CNTs of very small diameters (Supporting Information) showed similar behavior as larger crystals with the CNT (35,35) (Figure 3j–o, Figures S7 and S8). Different wrapping

https://doi.org/10.1021/acsnano.0c10027
ACS Nano 2021, 15, 6678–6683

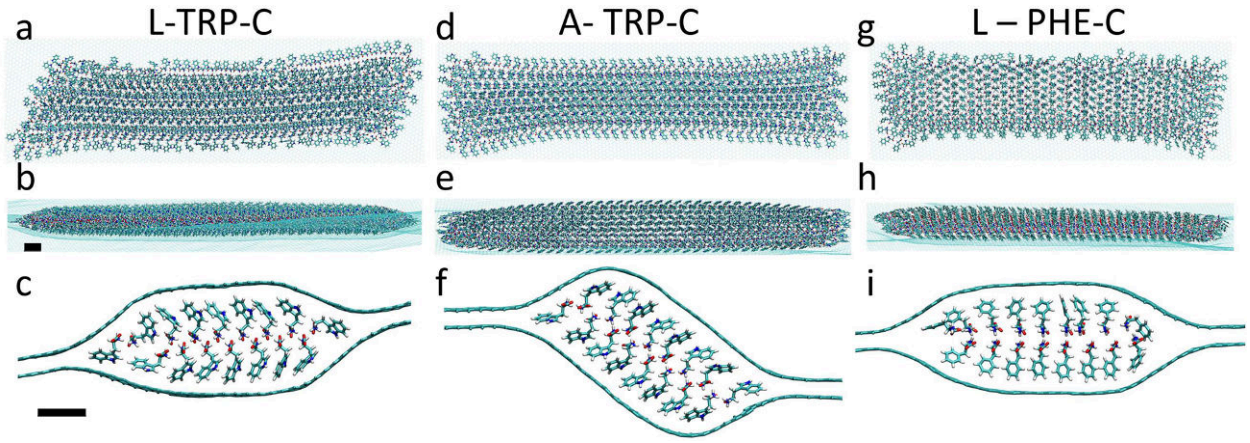


Figure 4. (a–c) Top, side, and single layer cross sectional views of the same L-TRP-C as in Figure 2a sandwiched between two circular graphene sheets (r = 30 nm) at 11 ns. (d–f) Top, side, and single layer cross sectional views of the same A-TRP-C crystal as in Figure 2d sandwiched between two graphene sheets at 12 ns. (g–i) Top, side, and single layer cross sectional views of same L-PHE-C in Figure 2f sandwiched between two graphene sheets at 11 ns. Scale bars represent 1 nm.

styles and speeds originated in different crystal structures.[33] Since A-TRP-C has a plane of symmetry at the center of its unit cell, which is absent in L-TRP-C,[34,35] A-TRP-C is flat and L-TRP-C is twisted in solution. Therefore, racemic crystals wrap around CNTs symmetrically, but enantiopure crystals are twisted (Supporting Information). However, their coupling energies are alike in both crystals (Figure S10).

Parts g–i of Figure 3 also show (94 ns) wrapping of L-PHE-C around this CNT, which was orthogonal to the aromatic zipper of the crystal. L-PHE-C became twisted and developed cracks (Supporting Information), revealing that it is more fragile than L-TRP-C. Similar cracking happens when the L-PHE-C zipper is aligned along CNT (see Figure S9). However, L-PHE-C is pretty stable on less deformed surfaces (Figure 2f,i). Larger crystals might form multilayer systems or other superstructures,[7,8] depending on the CNT and crystal relative positions. When the width of the crystals is significantly larger than the circumference of CNTs, we see formation of multilayer crystals around CNTs (Figure 3 j–l, S7 and S8). When the CNT is above the center of the crystal, the crystal folds around it, leading to the formation of a double bilayer (Figure 3 m–o, S7 and S8).

Biomolecular Crystals Intercalated in Graphene Cells. Finally, we have simulated L-TRP-C, A-TRP-C, and L-PHE-C (shown in Figure 2) intercalated between two circular graphene sheets (radius of r = 30 nm) without solvent. During the simulations, the biomolecular crystals diffused between the graphene sheets, but remained otherwise stable. Figure 4 shows that after ∼10 ns of simulations the crystals remained intact except at their edges, which became slightly deformed due to the pressure buildup from vdW-coupled graphenes.[36] The intracrystal coupling energies were practically not affected by the intercalation. Interestingly, the chirality of metabolite crystals somewhat affected their wrapping by graphene sheets. The enantiopure L-TRP-C and L-PHE-C crystals were wrapped by the two graphene sheets more symmetrically, where the midline between the sheets bisected the crystal through the zwitterion layer (Figures 4c,i). The racemic A-TRP-C crystal was wrapped in a tilted way, where the midline went through the crystal diagonally.

Stability of Biomolecular Crystals. The freely solvated metabolites predominantly bind to graphene through a $\pi-\pi$ coupling of its aromatic groups. On the other hand, crystalline metabolites predominantly bind with graphene through a $\sigma^{C-H}-\pi$ coupling, where the aromatic groups of the metabolites are orthogonal to the surfaces. Therefore, freely solvated metabolites have a stronger coupling with graphene than crystalline metabolites. On the other hand, crystalline metabolites have stronger binding with each other by $\pi-\pi$ coupling and the formation of hydrogen bonds. Since the intracrystal energies dominate, the adsorbed molecular crystals stay relatively intact.

To quantify these interactions, we have calculated intracrystal (within molecular crystal) and intercrystal (between crystal and nanomaterial) coupling energies (enthalpies) of individual amino acids to their neighborhoods (Figure S10). Intracrystal energies were broken down as (1) intralayer metabolites (E_{IRAL}) and (2) interlayer metabolites (E_{IERL}). We approximate the lattice energy (E_L) by the arithmetic mean of E_{IRAL} and E_{IERL}. We also calculate intercrystal interactions with the crystalline metabolites in direct contact of the nanosurface (E_{CN}). Finally, we calculated the interactions of solvated metabolites in direct contact with nanosurface (E_{SN}). In TRP (PHE) systems, $E_{IRAL} \approx 85$ (95) kcal/mol and $E_{IERL} \approx 55$ (29) kcal/mol between metabolites in the same and different layers, respectively, giving lattice energies of $E_L \approx 71$ (62) kcal/mol. These energies were practically unaffected by the presence of nanomaterials. In first principle studies, the lattice energies were E_L = 77.71 (73.26) kcal/mol for TRP (PHE) crystals,[37] in good agreement with our results. The intercrystal coupling energies were much weaker (E_{CN} = 4–8 kcal/mol), but they were slightly larger for amino acids freely adsorbed on nanomaterials (E_{SN} = 15–20 kcal/mol). TRP crystals have an enhanced rigidity of aromatic zippers caused by intracrystal interactions of the broader indole side groups.[32,33] On the other hand, PHE crystals have only a phenyl side group, which rotated frequently. Therefore, intracrystal interactions for PHE crystals were weaker (Figure S10), resulting in them cracking.

In summary, stable hybrid superstructures can be formed when biomolecular crystals are adsorbed (intercalated) on nanomaterials. Racemic crystals tend to adsorb in a straight manner, but enantiopure crystals naturally twist on nanosurfaces, deform them, and form helices (CNTs). These differences between enantiopure and racemic crystals can be

https://doi.org/10.1021/acsnano.0c10027
ACS Nano 2021, 15, 6678–6683

generalized to other chiral metabolites and biopolymers, and experimentally tested.[34,35] Combination of localized material properties originating from the biomolecular components with delocalized properties originating from the inorganic components can make these hybrid superstructures attractive for many applications.

METHODS

Graphene and CNTs were constructed with Nanotube Builder in VMD.[38] Phosphorene was based on a single unit cell of 4 phosphorus atoms,[39] which was propagated in two orthogonal directions. For simplicity, atoms on the nanosurfaces were not charged and not terminated by hydrogens. The polarizability of nanomaterials was neglected, even though armchair CNTs have a metallic character. L-TRP-C, A-TRP-C, and L-PHE-C were constructed using known crystallographic data.[29−31]

The MD simulations were performed with NAMD2.12,[40] using a CHARMM force field for metabolites and carbon atoms,[41] whereas phosphorus atoms used another force field.[39] The TIP3P water model was employed for explicit water simulations. Nonbonded interactions used the switching algorithm, with the switch-on distance at 10 Å and the switch-off at 12 Å. Nonbonded pair lists were used for atoms within 13.5 Å of each other, with the list updated every 20 steps. 1−4 nonbonded interactions were not scaled.

The Langevin dynamics was used with a damping constant of γ_{Lang} = 1 ps^{-1}, a piston period of 100 fs, a piston decay of 50 fs, and a piston temperature of 310 K. In the simulations of large crystals folding around CNTs, we choose γ_{Lang} = 0.01. The Velocity Verlet integrator was used to solve the equations of motion, with a time step of 2 fs. The SHAKE algorithm was used for hydrogens. Solvated simulations were done in the NPT ensemble with periodic boundary conditions applied, pressure of 1 atm, and under physiological conditions, [NaCl] = 0.15 M, with amino acids in zwitterionic forms and hydrogens excluded from the thermal bath. Simulations involving crystals in vacuum or sandwiched between graphene layers (without water) were done in the NVT ensemble, and periodic boxes 50% larger than the crystal-graphene systems. Except minimization, Particle Mesh Ewald summation[42] was used with a grid spacing of 1.0. All systems were minimized for at least 5,000 steps. During minimization and pre-equilibration, heavy atoms of amino acids and nanosurface atoms were constrained, but they well all released during the simulations. Data and snapshots were recorded every 10 ps.

The binding energies, with electrostatic and dispersion contributions, were calculated every 10 ps. Amino acids were classified as (1) molecules that were in the layer of the crystal in direct contact with the nanosurfaces and stayed intact (labeled as bottom), colored orange in Figures 1, 2 and 3; (2) molecules that were in the layer away from the nanosurfaces and stayed intact (labeled as top), colored red in Figures 1−3; and (3) molecules that dissolved from the crystal (labeled as free), colored gray in Figures 1−3. Intracrystal interaction energies were calculated between molecules within the same layer and between different layers, and normalized with respect to the number of molecules in each layer. The interaction energies between bottom amino acids and CNTs were normalized with respect to the number of amino acids that were within 4.5 Å of CNT at each time step. The coupling energies of free metabolites were normalized with respect to the number of amino acids that were within 4.5 Å of the nanosurfaces.

ASSOCIATED CONTENT

Supporting Information

Supporting Information The Supporting Information is available free of charge at https://pubs.acs.org/doi/10.1021/acsnano.0c10027.

Experimental procedures, Figures S1−S10, and movie descriptions (PDF)

100 ns dynamics of L-TRP-C adsorbed on phosphorene (AVI)

100 ns dynamics of L-TRP-C adsorbed on graphene (AVI)

100 ns dynamics of L-PHE-C adsorbed on graphene (AVI)

33 ns dynamics of L-TRP-C adsorbed on (18,18) carbon nanotube (AVI)

417 ns dynamics of L-TRP-C adsorbed on (35,35) carbon nanotube (AVI)

14 ns dynamics of A-TRP-C adsorbed on (35,35) carbon nanotube (AVI)

AUTHOR INFORMATION

Corresponding Author

Petr Král − *Department of Chemistry and Departments of Physics, Pharmaceutical Sciences, and Chemical Engineering, University of Illinois at Chicago, Chicago, Illinois 60607, United States;* orcid.org/0000-0003-2992-9027; Email: pkral@uic.edu

Author

Pavel Rehak − *Department of Chemistry, University of Illinois at Chicago, Chicago, Illinois 60607, United States*

Complete contact information is available at: https://pubs.acs.org/10.1021/acsnano.0c10027

Notes

The authors declare no competing financial interest.

REFERENCES

(1) Ross, C. A.; Poirier, M. A. Protein Aggregation and Neurodegenerative Disease. *Nat. Med.* **2004**, *10*, S10−S17.

(2) Rambaran, R. N.; Serpell, L. C. Amyloid Fibrils Abnormal Protein Assembly. *Prion* **2008**, *2*, 112−117.

(3) Knowles, T. P. J.; Vendruscolo, M.; Dobson, C. M. The Amyloid State and Its Association with Protein Misfolding Diseases. *Nat. Rev. Mol. Cell Biol.* **2014**, *15*, 384−396.

(4) Do, T. D.; Bowers, M. T. Diphenylalanine Self-Assembly: Novel Ion Mobility Methods Showing the Essential Role of Water. *Anal. Chem.* **2015**, *87*, 4245−4252.

(5) Do, T. D.; de Almeida, N. E. C.; LaPointe, N. E.; Chamas, A.; Feinstein, S. C.; Bowers, M. T. Amino Acids Metaclusters: Implications of Growth Trends on Peptide Self-Assembly and Structure. *Anal. Chem.* **2016**, *88*, 868−876.

(6) Wei, G.; Su, Z.; Reynolds, N. P.; Arosio, P.; Hamley, I. W.; Gazit, E.; Mezzenga, R. Self-Assembling Peptide and Protein Amyloids: From Structure to Tailored Function in Nanotechnology. *Chem. Soc. Rev.* **2017**, *46*, 4661−4708.

(7) Patra, N.; Wang, B.; Král, P. Nanodroplet Activated and Guided Folding of Graphene Nanostructures. *Nano Lett.* **2009**, *9*, 3766−3771.

(8) Patra, N.; Song, Y.; Král, P. Self-Assembly of Graphene Nanostructures on Nanotubes. *ACS Nano* **2011**, *5*, 1798−1804.

(9) Sen, S.; Han, Y.; Rehak, P.; Vuković, L.; Král, P. Computational Studies of Micellar and Nanoparticle Nanomedicines. *Chem. Soc. Rev.* **2018**, *47*, 3849−3860.

(10) Sen, S.; Vuković, L.; Král, P. Computational Screening of Nanoparticles Coupling to Aβ40 Peptides and Fibrils. *Sci. Rep.* **2019**, *9*, 17804−17811.

(11) Rajesh, C.; Majumder, C.; Kawazoe, Y. A Theoretical Study on the Interaction of Aromatic Acids with Graphene and Single Walled Carbon Nanotube. *J. Chem. Phys.* **2009**, *130*, 124911−124916.

(12) Panigrahi, S.; Bhattacharya, A.; Banerjee, S.; Bhattacharyya, D. Interaction of Nucleobases with Wrinkled Graphene Surface: Dispersion Corrected and AFM Studies. *J. Phys. Chem. C* **2012**, *116*, 4374−4379.

(13) Camden, A. N.; Barr, S. A.; Berry, R. J. Simulations of Peptide-Graphene Interactions in Explicit Water. *J. Phys. Chem. B* **2013**, *117*, 10691−10697.
(14) Umadevi, D.; Sastry, G. N. Impact of the Chirality and Curvature of Carbon Nanostructures on Their Interaction with Aromatic and Amino Acids. *ChemPhysChem* **2013**, *14*, 2570−2578.
(15) Umadevi, D.; Panigrahi, S.; Sastry, G. N. Noncovalent Interaction of Carbon Nanostructure. *Acc. Chem. Res.* **2014**, *47*, 2574−2581.
(16) Tavassoli Larijani, H.; Darvish Ganji, M.; Jahanshahi, M. Trends of Amino Acid Adsorption onto Graphene Oxide Surfaces: A Dispersion Corrected DFT Study. *RSC Adv.* **2015**, *5*, 92843−92857.
(17) Yang, Z.; Ge, C.; Liu, J.; Chong, Y.; Gu, Z.; Jimenez-Cruz, C. A.; Chai, Z.; Zhou, R. Destruction of Amyloid Fibrils by Graphene through Penetration and Extraction of Peptides. *Nanoscale* **2015**, *7*, 18725−18737.
(18) Ghadari, R. A Study on the Interaction of Amino Acids with Nitrogen Doped Graphene; Docking, MD Simulation, and QM/MM Studies. *Phys. Chem. Chem. Phys.* **2016**, *18*, 4352−4361.
(19) Mallineni, S. S. K.; Shannahan, J.; Raghavendra, A. J.; Rao, A. M.; Rao, A. M.; Brown, J. M.; Podila, R. Biomolecular Interactions and Biological Responses of Emerging Two-Dimensional Materials and Aromatic Amino Acid Complexes. *ACS Appl. Mater. Interfaces* **2016**, *8*, 16604−16611.
(20) Larijani, H. T.; Jahanshahi, M.; Ganji, M. D.; Kiani, M. H. Computational Studies on the Interactions of Glycine Amino Acids with Graphene, h-BN and h-SiC Monolayers. *Phys. Chem. Chem. Phys.* **2017**, *19*, 1896−1908.
(21) Zou, X.; Wei, S.; Jasensky, J.; Xiao, M.; Wang, Q.; Brooks, C. L.; Chen, Z. Molecular Interactions between Graphene and Biological Molecules. *J. Am. Chem. Soc.* **2017**, *139*, 1928−1936.
(22) Božinovski, D. K.; Petrović, P. V.; Belić, M. R.; Zarić, S. D. Insight into the Interactions of Amyloid β-Sheets with Graphene Flakes: Scrutinizing the Role of Aromatic Residues in Amyloids That Interact with Graphene. *ChemPhysChem* **2018**, *19*, 1226−1233.
(23) Titov, A.; Král, P.; Pearson, R. Sandwiched Graphene-Membrane Superstructures. *ACS Nano* **2010**, *4*, 229−234.
(24) Chan, H.; Král, P. Nanoparticles Self-Assembly within Lipid Bilayers. *ACS Omega* **2018**, *3*, 10631−10637.
(25) Oliveira, S. F.; Bisker, G.; Bakh, N. A.; Gibbs, S. L.; Landry, M. P.; Strano, M. S. Protein Functionalized Carbon Nanomaterials for Biomedical Applications. *Carbon* **2015**, *95*, 767−779.
(26) Roxbury, D.; Jena, P. V.; Shamay, Y.; Horoszko, C. P.; Heller, D. A. Cell Membrane Proteins Modulate the Carbon Nanotube Optical Bandgap via Surface Charge Accumulation. *ACS Nano* **2016**, *10*, 499−506.
(27) Yaari, Z.; Cheung, J. M.; Baker, H. A.; Frederiksen, R. S.; Jena, P. V.; Horoszko, C. P.; Jiao, F.; Scheuring, S.; Luo, M.; Heller, D. A. Nanoreporter of an Enzymatic Suicide Inactivation Pathway. *Nano Lett.* **2020**, *20*, 7819−7827.
(28) Geim, A. K.; Grigorieva, I. V. van der Waals Heterostructures. *Nature* **2013**, *499*, 419−425.
(29) Hübschle, C. B.; Messerschmidt, M.; Luger, P. Crystal Structure of DL-Tryptophan at 173 K. *Cryst. Res. Technol.* **2004**, *39*, 274−278.
(30) Görbitz, C. H.; Törnroos, K. W.; Day, G. M. Single-Crystal Investigation of L-Tryptophan with Z′ = 16. *Acta Crystallogr., Sect. B: Struct. Sci.* **2012**, *B68*, 549−557.
(31) Mossou, E.; Teixeira, S. C. M.; Mitchell, E. P.; Mason, S. A.; Adler-Abramovich, L.; Gazit, E.; Forsyth, V. T. The Self-Assembling Zwitterionic form of L-Phenylalanine at Neutral pH. *Acta Crystallogr., Sect. C: Struct. Chem.* **2014**, *C70*, 326−331.
(32) Shaham-Niv, S.; Rehak, P.; Vuković, L.; Alder-Abramovich, L.; Král, P.; Gazit, E. Formation of Apoptosis-Inducing Amyloid Fibrils by Tryptophan. *Isr. J. Chem.* **2017**, *57*, 729−737.
(33) Bera, S.; Xue, B.; Rehak, P.; Jacoby, G.; Ji, W.; Shimon, L. J. W.; Beck, R.; Král, P.; Cao, Y.; Gazit, E. Self-Assembly of Aromatic Amino Acid Enantiomers into Supramolecular Materials of High Rigidity. *ACS Nano* **2020**, *14*, 1694−1706.
(34) Yeates, T. O.; Kent, S. B. H. Racemic Protein Crystallography. *Annu. Rev. Biophys.* **2012**, *41*, 41−61.
(35) Kent, S. B. H. Racemic & Quasi-Racemic Protein Crystallography Enabled by Chemical Protein Synthesis. *Curr. Opin. Chem. Biol.* **2018**, *46*, 1−9.
(36) Ghodsi, S. M.; Sharifi-Asl, S. S.; Rehak, P.; Král, P.; Megaridis, C. M.; Shahbazian-Yassar, R.; Shokuhfar, T. Assessment of Pressure and Density of Confined Water in Graphene Liquid Cells. *Adv. Mater. Interfaces* **2020**, *7*, 1901727−1901736.
(37) Červinka, C.; Fulem, M. Cohesive Properties of the Crystalline Phases of Twenty Proteinogenic α-Aminoacids from First-Principles Calculations. *Phys. Chem. Chem. Phys.* **2019**, *21*, 18501−18515.
(38) Humphrey, W.; Dalke, A.; Schulten, K. VMD: Visual Molecular Dynamics. *J. Mol. Graphics* **1996**, *14*, 33−38.
(39) Sresht, V.; Pádua, A. A. H.; Blankschtein, D. Liquid-Phase Exfoliation of Phosphorene: Design Rules from Molecular Dynamics Simulations. *ACS Nano* **2015**, *9*, 8255−8268.
(40) Phillips, J. C.; Braun, R.; Wang, W.; Gumbart, J.; Tajkhorshid, E.; Villa, E.; Chipot, C.; Ske el, R. D.; Kalé, L.; Schilten, K. Scaleable Molecular Dynamics with NAMD. *J. Comput. Chem.* **2005**, *26*, 1781−1802.
(41) MacKerell, A. D.; Bashford, D.; Bellot, M.; Dunbrack, R. L.; Evanseck, J. D.; Field, M. J.; Fischer, S.; Gao, J.; Guo, H.; Ha, S.; Joseph-McCarthy, D.; Kunchnir, L.; Kuczera, K.; Lau, F. T. K.; Mattos, C.; Michnick, S.; Ngo, T.; Nguyen, D. T.; Prodhom; B. Reiher, W. E.; et al. All-Atom Empirical Potential for Molecular Modeling and Dynamics Studies of Proteins. *J. Phys. Chem. B* **1998**, *102*, 3586−3616.
(42) Darden, T.; York, D.; Pedersen, L. Particle Mesh Ewald: An n·log(n) Method for Ewald Sums in Large Systems. *J. Chem. Phys.* **1993**, *98*, 10089−10092.

https://doi.org/10.1021/acsnano.0c10027
ACS Nano 2021, 15, 6678−6683